PROCEEDINGS, 42nd Workshop on Geothermal Reservoir Engineering
Stanford University, Stanford, California, February 13-15, 2017
SGP-TR-212

Numerical Analysis of Transient Steam-Water Two-Phase Flow in Geothermal Production Wells with Multiple Feed Zones

Keisuke Yamamura[1], Ryuichi Itoi[1], Toshiaki Tanaka[1] and Takaichi Iwasaki[2]

[1]Department of Earth Resources Engineering, Faculty of Engineering, Kyushu University, Fukuoka 819-0395, Japan

[2]Mitsubishi Materials Co., Japan

k722eisuke@gmail.com

Keywords: wellbore simulator, cyclic behavior, unsteady two-phase flow, numerical simulation, flow instability boundary map

ABSTRACT

Geothermal production wells sometimes show oscillations of wellhead pressure and flow rate when they are completed with multiple feed zones. This instability of the production leads to problems of power plant operation, such as lack of steam supply and unstable turbine inlet pressure. In the worst-case scenario, steam production of the well may cease. Its mechanism, however, has not been well understood. In this study, we developed a numerical model of transient steam-water two-phase flow in a geothermal production well. This wellbore model is coupled with a reservoir model so we can treat flow rate change with time from the reservoir into the wellbore and deal with a well with multiple feed zones. We use a homogeneous model for steam-water mixture flow in a wellbore and related conservation equations. The simulation results show that the oscillation of flow rate in a wellbore begins to appear as the temperature difference of the fluids between feed zones becomes large. This also shows that the oscillation is generated by interactions among pressure, pressure drop, and specific enthalpy in a wellbore.

1. INTRODUCTION

Stable production of wells is an essential task for geothermal reservoir operation and steady power generation of plants. Geothermal energy is accessible round the clock, and is thus often considered a base load source of power generation. Geothermal production wells can be constructed by penetrating fractured zones at different depths to enhance productivity of steam. However, some have oscillation of wellhead pressure and flow rate (Grant et al., 1979; Iwata et al., 2002; Itoi et al., 2013). These wells eventually cease steam production because the wellhead pressure drops below production header pressure. These unstable behaviors of the well are not favorable for reservoir management, so the cause of the oscillation must be examined. However, there are few observed data in wells during their cyclic behavior because of the difficulty of a flowing survey. Therefore, there is a need for simulation studies with a numerical model of transient steam-water two-phase flow in geothermal production wells.

Simulation studies were conducted to evaluate the effect of permeability-thickness (kh) of reservoirs on flow in wellbores (Itoi et al., 2013; Katayama et al., 2013; Inagaki et al., 2014). They simulated the fluctuation of wellhead pressure and flow rate and analyzed its mechanism. These works, however, used the modified simulation program WELBORE, which was originally developed by Miller (Miller, 1980). Their simulator cannot handle change in wellbore radius nor inclined wells, which is common for production wells. The simulator T2Well can simulate transient non-isothermal, two-phase and multi-component flow in wellbore-reservoir systems (Pan and Oldenburg, 2014). This simulator computes fluid flows both in the wellbore and reservoir simultaneously. This has been developed and used mainly in the simulation of carbon capture storage problems and cannot treat high-enthalpy fluid (Pruess, 2008; Pan et al., 2009). We developed a numerical model for transient, two-phase high-enthalpy fluid flow in geothermal production wells (Yamamura et al., 2016a). This simulator can handle an inclined wellbore of variable well radius. However, it cannot treat a wellbore with multiple feed zones, so we included sink-source terms in a new wellbore model to handle the oscillation of production rate. Our simulated results show an unstable behavior (Yamamura et al., 2016b). We found that substantial fluid temperature differences between the shallow and deep reservoir causes oscillation of the production rate. This simulator uses the linearized equation of state, which has a problem of mass error (Miller, 1980). Consequently, density error accumulated within an unstable calculation so that the simulator still could not run a long-term simulation. This meant that simulation time was not sufficient, so production did not stop after oscillation, whose mechanism is not well understood. In this study, we applied a new method to calculate density accurately. Long-period simulations were carried out to understand the mechanism of the unstable behavior and we introduced a flow instability boundary map via the numerical experiment.

2. SIMULATION MODEL

We developed a computer program that simulates one-dimensional homogeneous transient flow of liquid-water, single-phase and steam-water two-phase in an inclined wellbore with variable diameters and multiple feed zones.

2.1 Wellbore Model

2.1.1 Basic Equations

A mathematical model consists of conservation equations for mass, momentum and energy, which are described below.

$$\frac{\partial \rho}{\partial t}+\frac{\partial \rho u}{\partial z}=\frac{M'}{V} \tag{1}$$

$$\frac{\partial u}{\partial t}+u\frac{\partial u}{\partial z}=-\frac{1}{\rho}\frac{\partial P}{\partial z}-\frac{1}{2}\left(K+\frac{\lambda}{D}\right)u|u|-g\cos\theta \tag{2}$$

$$\frac{\partial \rho H}{\partial t}+\frac{\partial \rho H u}{\partial z}=\frac{\partial P}{\partial t}+q+\frac{M'H'}{V}, \tag{3}$$

where ρ is average density (kg/m^3), u is velocity (m/s), P is pressure (Pa), θ is the wellbore angle measured from the vertical (°), K is the shape pressure loss factor (1/m), H is total energy per unit mass (J/kg), h is specific enthalpy (J/kg), q is heat transfer per unit volume (W/m^3), t is time (s), and z is the vertical distance (m). The first term on the right side of Eq. (1) and third term on the right side of Eq. (3) are sink-source terms. We can represent fluid flow between the wellbore and reservoir by these terms.

2.1.2 Constitutive Equations

λ is the friction factor of a pipe (-) and is calculated by Karman's formula (Nakayama, 2007):

$$\lambda=\frac{1}{\left(1.14+2\log\frac{D}{\varepsilon}\right)^2}, \tag{4}$$

where ε is surface roughness of a pipe (m) and D is wellbore diameter (m). In a two-phase flow region, the friction factor is given as 1.1 times that of a single-phase region. For this calculation, the slip between the phases was assumed to be zero and the friction factor was constant.

The shape loss factor must be evaluated in a different way depending on the direction of flow with respect to the change in diameter of the wellbore (Japan Society of Mechanical Engineers, 1979), as follows.

For increasing well diameter,

$$K=\left(1-\frac{A_1}{A_2}\right)^2\frac{1}{\Delta z}. \tag{5}$$

For decreasing well diameter,

$$K=\left\{0.5-0.7\left(\frac{A_1}{A_2}\right)^2+0.2\left(\frac{A_1}{A_2}\right)^2\right\}\frac{1}{\Delta z}, \tag{6}$$

where A_1 is the smaller cross-sectional area at the junction (m^2), A_2 is the larger cross-sectional area at that junction (m^2), and Δz is the grid length of the wellbore (m).

The state equation is needed to relate state quantities P, h and ρ.

$$\frac{\partial \rho}{\partial P}=\left.\frac{\partial \rho}{\partial P}\right|_h+\left.\frac{\partial \rho}{\partial h}\right|_P\frac{dh}{dP}. \tag{7}$$

The void fraction is calculated by Smith's formula (Smith, 1969-70) as

$$\alpha=\left\{1+\frac{v_l}{v_g}\phi\left(\frac{1}{x}-1\right)+\frac{v_l}{v_g}(1-\phi)\left(\frac{1}{x}-1\right)\sqrt{\frac{\frac{v_g}{v_l}+\phi\left(\frac{1}{x}-1\right)}{1+\phi\left(\frac{1}{x}-1\right)}}\right\}^{-1}, \tag{8}$$

where v_l is the specific volume of water (m^3/ kg), v_g is the specific volume of steam (m^3/ kg), x is steam quality (-), and 0.4 is given for the parameter ϕ.

2.2 Reservoir Model

The reservoir model assumes water single-phase flow or steam-water two-phase flow in a radial coordinate system of constant thickness and isotropic rock properties of porous media. Fluid flow obeys Darcy's law. The corresponding mass flow rate M (kg/s) from the reservoir into the wellbore at a feed zone is then calculated as

$$M' = \frac{2\pi k h \rho}{\mu} \frac{P_{re} - P_{fz}}{\ln r_{re}/r_w}, \tag{9}$$

where kh is permeability-thickness of the reservoir (m^3), P_{re} is reservoir pressure (Pa), P_{fz} is pressure at the feed zone (Pa), r_{re} is the outer boundary radius of reservoir (m), r_w is wellbore radius (m), μ is the coefficient of dynamic viscosity (Pa·s), and ρ is density (kg/m^3).

2.3 Numerical Approach

We used the finite difference method for discretization of basic equations, which leads to a simultaneous linear equation with respect to the pressure difference (Yamamura et al., 2016a). Eq.(7) is discretized by applying the semi implicit method as

$$\Delta\rho^{n+1} = \frac{\rho\left(P^{n+1}+\Delta P^{n+1}, h^n+\Delta h^{n+1}\right)-\rho\left(P^n, h^{n+1}+\Delta h^{n+1}\right)}{\Delta P^{n+1}}\Delta P^{n+1} + \frac{\rho\left(P^n, h^{n+1}+\Delta h^{n+1}\right)-\rho\left(P^n, h^n\right)}{\Delta h^{n+1}}\Delta h^{n+1}, \tag{10}$$

where superscripts n and n+1 indicate previous and current times, respectively, and Δ indicates change between n and n+1. ΔP^{n+1} and Δh^{n+1} are used to calculate the density accurately. However, they are unknown parameters at n so the iterative calculation is introduced to obtain them. Figure 1(a) presents a conceptual model of fluid flows in the reservoir and wellbore and Fig. 1(b) shows the flowchart of calculation.

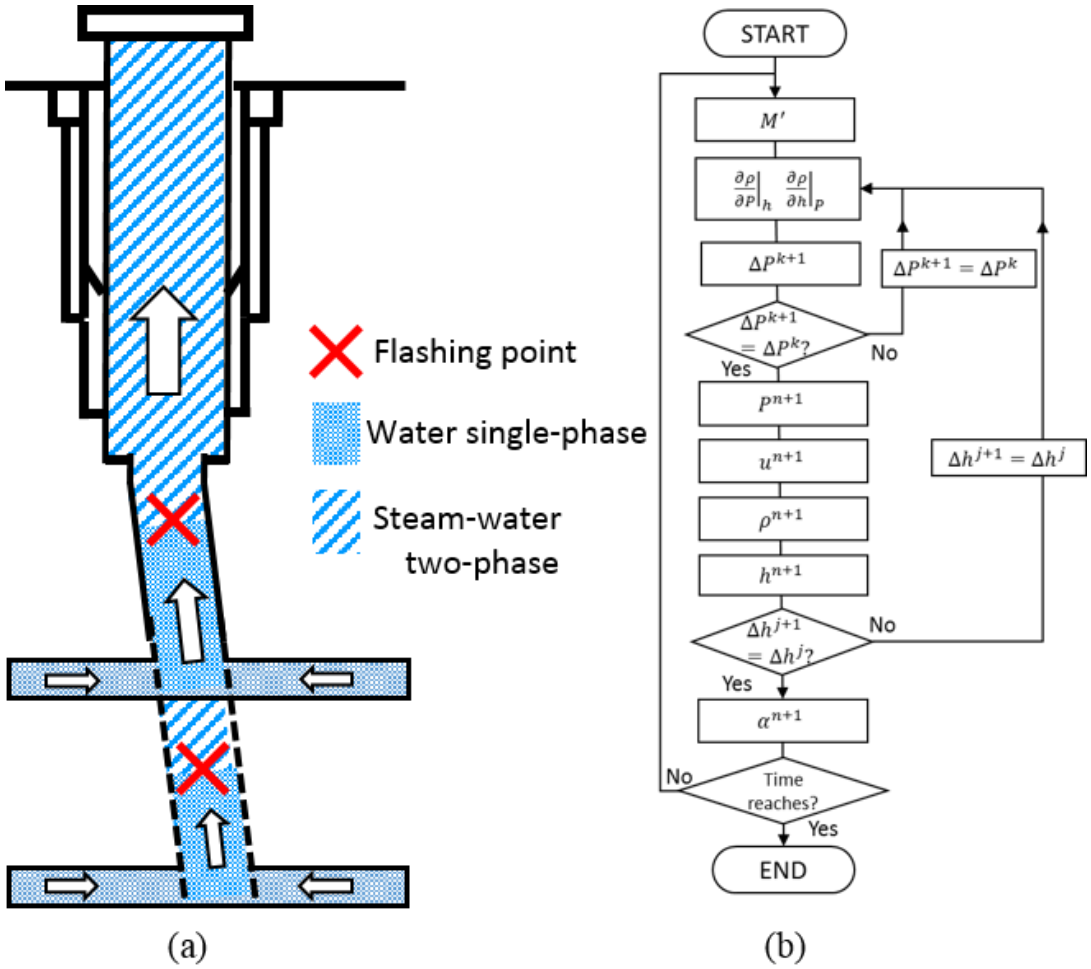

Figure 1: (a) Conceptual Model of fluid flow in reservoir and wellbore (b) Flowchart of calculation

3. NUMERICAL SIMULATION

We conducted simulations to understand the unstable behavior in the wellbore. We assumed a vertical well of 2000-m depth and diameter 0.2 m. Reservoir parameters are summarized in Table 1. These data were taken from a production well in a geothermal field of northern Japan. We varied shallow reservoir temperature T_{res} in each simulation to examine the effect of the temperature difference between feed zones ΔT_{re} on wellbore flow. The unsteady state calculation was conducted for 8 h.

Table 1: Parameters of each reservoir

Reservoir	Depth(m)	Pressure(bar)	Temperature (℃)	kh (darcy·m)	Outer radius (m)
Deep	2000	45	260	4.0	1000
Shallow	1400	100	160～250	1.0	1000

3.1 Boundary Conditions

Boundary conditions of Dirichlet type are used to specify pressure or flow rate at the boundary. Specifically, the flow rate at the well bottom is fixed to zero and the boundary at the well bottom is regarded as closed. Wellhead pressure was fixed at 7 bar throughout the simulation period.

3.2 Initial Conditions

Pressure and temperature profiles in the wellbore under steady state were determined by a wellbore flow model (Katayama, 2011) and were taken as initial conditions. This steady flow model assumes that wellbore flow is stable and that enthalpy remains constant between each feed zone. In these calculations, we did not consider heat transfer from the wellbore to the surrounding formation. Total energy equals specific enthalpy because the kinetic and potential energies are negligibly small compared to specific enthalpy.

3.2 Simulation Results

3.2.1 The difference of the wellbore flow due to the temperature difference between the shallow and deep feed zones

Figure 2(a) shows the change of production rate with time when T_{res} was 230, 240, and 250 °C. All production rates were stable throughout the simulation period. In contrast, Fig. 2(b) shows changes of that rate for T_{res} < 230 °C, all of which were unstable. At 220 °C, the production rate showed cyclic change, and production halted after 7 h. From these results, production becomes unstable when ΔT_{re} is large.

3.2.2 Profile of specific enthalpy in the well with time

We now address the result for T_{res} = 220 °C and deep reservoir temperature T_{red} = 260 °C. Specific enthalpies of saturated water of each reservoir h_{res} and h_{red} were 944 and 1135 kJ/kg, respectively. Figure 3(a) shows the profile of specific enthalpy in the well with time t = 17,200–20,030 s. Upward flow persisted until production stopped and high enthalpy fluid from the deep reservoir filled the deeper part of the wellbore, between deep feed zone FZd and shallow feed zone FZs. Consequently, the profile of specific enthalpy was constant at 1135 kJ/kg in the deeper part. In contrast, the profile in the shallower part of the wellbore (shallower than FZs) changed with time. High-enthalpy fluid from the deeper part of the wellbore mixed with low-enthalpy fluid from the shallow reservoir at FZs, and the mixed specific enthalpy at FZs h_{mix} changed. Thus, this fluid with specific enthalpy varying with time at FZs was transported to the shallower part of the wellbore by the upward flow. Consequently, the profile of specific enthalpy in the shallower part changed and the depth of the same specific enthalpy moved upward with time. When ΔT_{re} was large and the flow rate showed unstable behavior, the wellbore flow also had unstable behavior. Figure 3(b) presents the profile of specific enthalpy in the wellbore as a function of time. The contour represents the value of specific enthalpy at each depth with time. High enthalpy fluid of 1135 kJ/kg exists in the deeper part of the wellbore and holds the same value. This high enthalpy fluid at FZs is transported towards the wellhead periodically. This high enthalpy fluid flows upward slowly at the depths of between 1400m and 1200m and then flows upward rapidly at the depths of between 1200m and wellhead. The contours do not change after 7 h because the production ceased as shown in Fig. 2(b) and the propagation of specific enthalpy also ended.

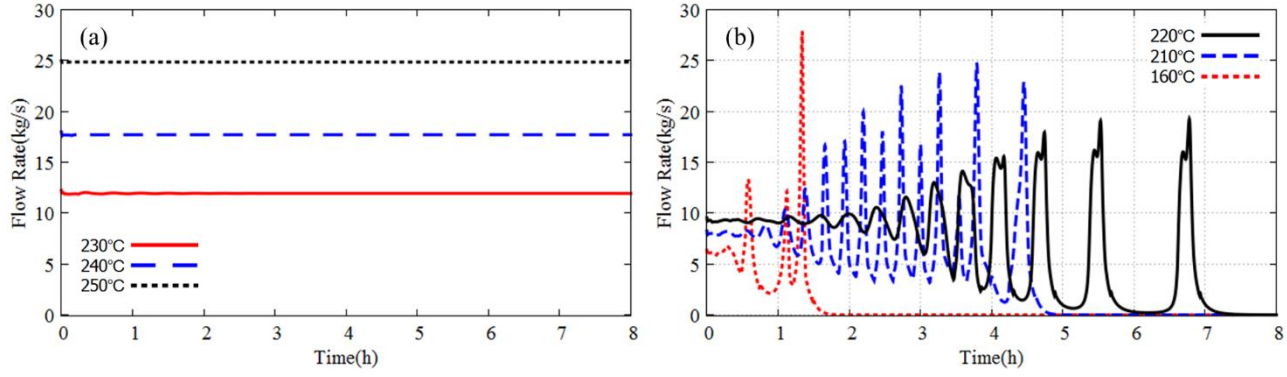

Figure 2: Production rate change with time (a) T_{res} = 230, 240, and 250 °C; (b) T_{res} = 160, 210, and 220 °C

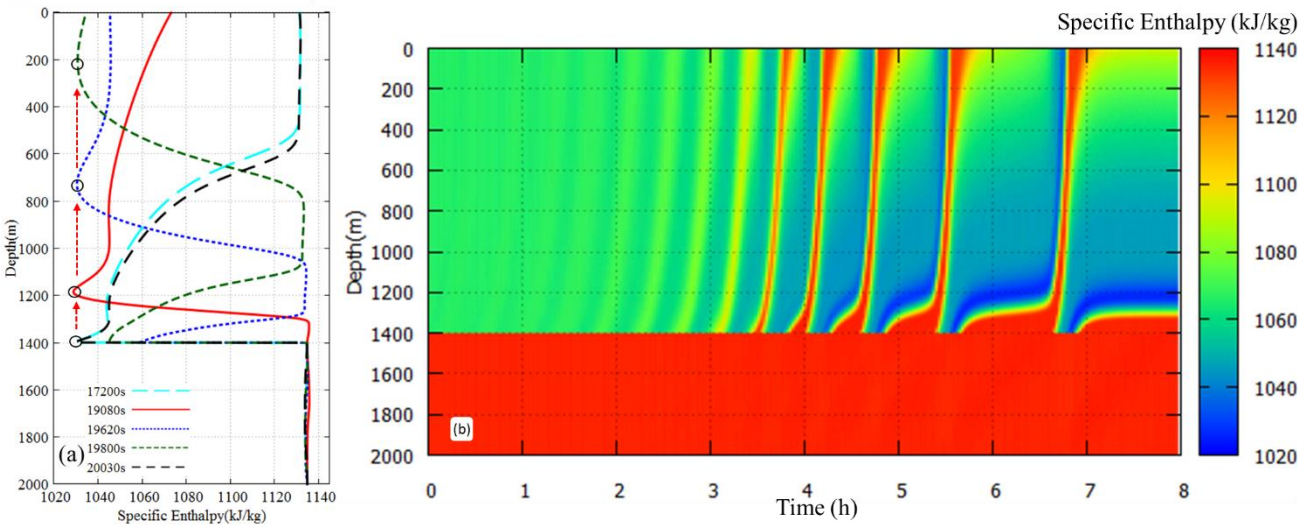

Figure 3: Profile of specific enthalpy (a) t = 17200, 19080, 19620, 19800, and 20030 s; (b) contour map as a function of time

3.2.3 Relationship between pressures in shallow and deep feed zones

Figure 4(a) shows pressure with time at the shallow feed zone P_{fzs} and deep feed zone P_{fzd}, and Fig. 4(b) reveals the relationship between these two types of pressure. The two oscillate with the same phase. Thus, the two pressures had positive correlation and were unique, with their correlation coefficient 0.9988. Now, we define total pressure loss ΔP_{fzd}^{fzs} between P_{fzs} and P_{fzd}; this relationship is

$$P_{fzd} = P_{fzs} + \Delta P_{fzd}^{fzs}. \tag{11}$$

Normally, within total pressure loss, that caused by elevation change contributes 80%–95%, so friction and acceleration losses are normally negligible (Brill and Mukhmerjee, 1999). Therefore, Eq. (11) can be rearranged as

$$P_{fzd} = P_{fzs} + \int_{fzd}^{fzs} \rho_i g \Delta z_i dz, \tag{12}$$

where Δz is grid size (m) and i is grid number (-). The second term on the right side represents the fluid weight per unit area of the deeper part of the wellbore. Density is a function of pressure and specific enthalpy, and density in Eq. (9) increases with pressure or a decrease in specific enthalpy. As mentioned in Section 3.2.2, the profile of specific enthalpy in the deeper part of the wellbore is constant. Hence, the density in that is a function of pressure only. Therefore, the second term on the right side increases with P_{fzs} so that P_{fzs} and P_{fzd} are unique in Eq. (12), and P_{fzd} is approximated by a quadratic function:

$$P_{fzd} = -0.0451 P_{fzs}^2 + 5.2676 P_{fzs} - 54.762, \tag{13}$$

where the units of P_{fzs} and P_{fzd} are bar.

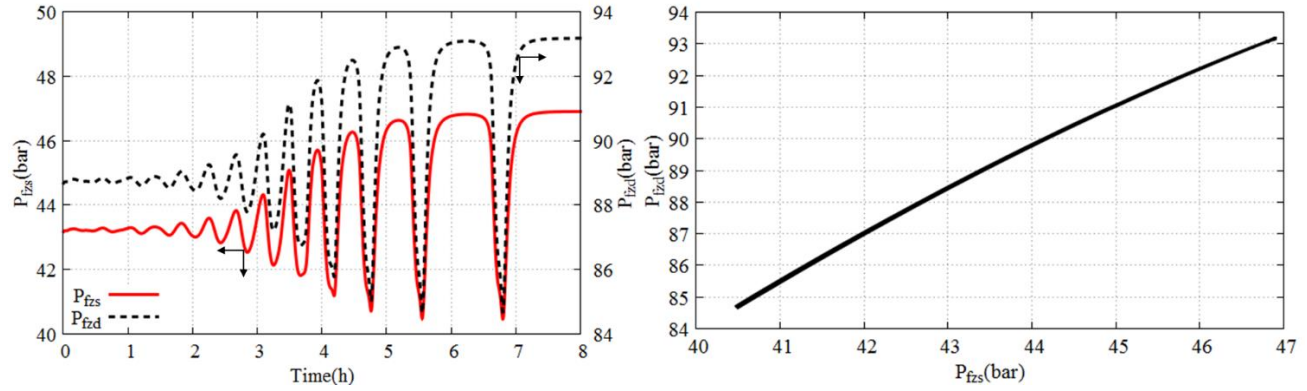

Figure 4: (a) Changes of P_{fzs} and P_{fzd} with time; (b) P_{fzs} versus P_{fzd} with time

3.2.4 Relationship between pressure and specific enthalpy at shallow feed zone

Figure 5(a) shows P_{fzs} and h_{mix} with time. They oscillated with the same phase. Equation (3) determines specific enthalpy change with time. The first and second term on its right side are negligibly small, because specific enthalpy change as a result of pressure variation is small and heat transfer was set to zero in this calculation. As a result, h_{mix} is determined by the second term on the left side and third term on the right side. This indicates that change of h_{mix} is caused by mixing with high-enthalpy fluid from the deeper part of the wellbore and low-enthalpy fluid from the shallow reservoir. Therefore, h_{mix} is

$$h_{mix} = R_s h_{res} + (1 - R_s) h_{red}, \tag{14}$$

$$Rs = \frac{M_{fzs}}{M_{fzs} + M_{fzd}}, \tag{15}$$

where h_{res} and h_{red} are specific enthalpies (kJ/kg) of saturated water of the shallow and deep reservoir fluid, respectively, and M_{fzs} and M_{fzd} are mass flow rates (kg/s) from the shallow and deep reservoir. Rs represents the ratio of M_{fzs} to total flow rate in the two reservoirs. When $M_{fzs} < 0$, Rs = 0 and when $M_{fzd} < 0$, Rs = 1. Figure 5(b) shows the relationship between P_{fzs} and Rs with time. Rs = 0 when P_{fzs} is ≥ 45 bar. This is because P_{res} = 45 bar and M_{fzs} would be negative from Eq. (9). This means that the low-enthalpy water does not mix at FZs, so h_{mix} remains constant at 1135 kJ/kg in Fig. 3. Consequently, h_{mix} has an upper limit of 1135 kJ/kg in Fig. 5(a). In contrast, Rs increases with a decrease in P_{fzs} when P_{fzs} is < 45 bar, and they are unique. Equations (9) and (15) can be rearranged as

$$Rs = \frac{r_s P_{fzs} - r_s P_{res}}{r_s P_{fzs} + P_{fzd} - r_s P_{res} - P_{red}}, \tag{16}$$

$$r_s = \frac{(kh)_{res}}{(kh)_{red}} \frac{\rho_{res}\mu_{red}}{\rho_{red}\mu_{res}}. \tag{17}$$

r_s, P_{res} and P_{red} are constant in this calculation, so Rs is a function of P_{fzs} and P_{fzd}. Substituting Eq. (13) into Eq. (16) gives Rs as a function of P_{fzs}:

$$Rs = \frac{3.589 P_{fzs} - 161.49}{-0.0451 P_{fzs}^2 + 8.856 P_{fzs} - 316.26}. \tag{18}$$

The derivative of Eq. (18) is negative, so Rs increases with a decrease in P_{fzs}. Therefore, Eq. (14) indicates that h_{mix} increases with a decrease in P_{fzs}, and they are unique.

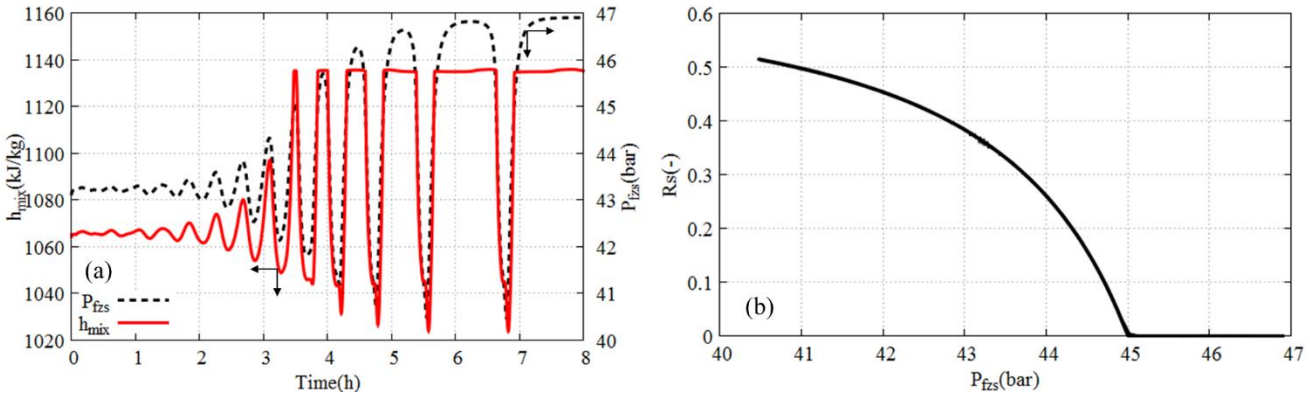

Figure 5: (a) Changes of h_{mix} and P_{fzs} with time; (b) P_{fzs} versus Rs with time

3.2.5 Relationship between pressure in shallow feed zone and average density in shallow part of the wellbore

We define the average density ρ_{aves} of the shallower part of the wellbore between the wellhead and FZs. In the same manner as Eqs. (11) and (12), total pressure loss in the shallower part of the wellbore can approximate pressure loss from elevation change. The equation is

$$P_{fzs} = P_{wh} + \rho_{aves} g \Delta z_s, \tag{19}$$

where Δz_s is the depth difference between FZs and wellhead. Figure 6 shows changes of P_{fzs} and ρ_{aves} with time; they oscillate at nearly the same phase. This is because P_{wh} is constant in the calculation so that P_{fzs} and ρ_{aves} are unique and P_{fzs} increases with ρ_{aves}. Therefore, ρ_{aves}change alters P_{fzs}, which in turn modifies Rs and h_{mix} as mentioned in Section 3.2.4.

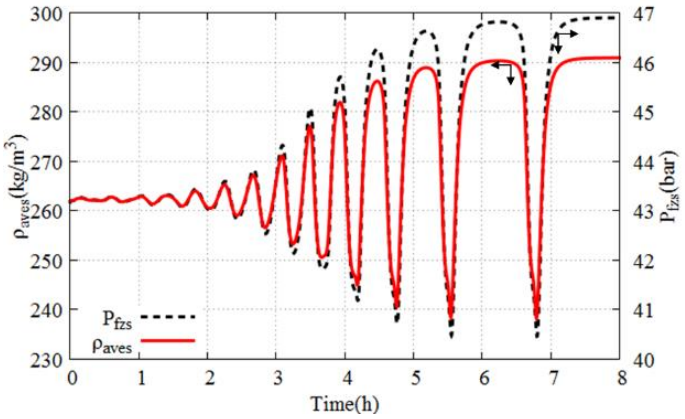

Figure 6: Changes of P_{fzs} and $\rho_{aves}$with time

3.2.6 Relationship between density change and propagation of specific enthalpy

Next, we consider the change of ρ_{aves}. Figure 7 shows the profile of specific enthalpy and density in the well with time during t = 17200–20030 s. This period corresponds to one cycle of the oscillation. P_{fzs}, h_{mix} and ρ_{aves} had small values at 17200 and 20030 s as Fig. 6 shows. Two-phase fluid from the deeper part of the wellbore changed to the water single phase at FZs, because low-enthalpy fluid from the shallow feed zone mixed with high-enthalpy fluid. After this time, h_{mix} increased with P_{fzs}. Therefore, high-enthalpy fluid from the deeper part of the wellbore remained two-phase at FZs and flowed upward to form a two-phase region between depths 1400–1250 m at 19080 s. There was low-enthalpy fluid, however, above this high-enthalpy flow so that the water single column remained between 1250 and 1180 m. This remaining water single column transformed to two-phase when high-enthalpy fluid reached a depth around 1200 m. This disappearance of the water single column between 1250 and 1180 m depths reduced ρ_{aves}, and the flow rate increased rapidly (Fig. 7(b)). Thus, this decrease in ρ_{aves} also reduced P_{fzs} so that low-temperature fluid entered the wellbore at FZs to form a water single column at FZs again at 19620 and 19800 s. Then, profiles of density and specific enthalpy at 20030 s returned to that at 17200s. This was one cycle of the oscillation. This cyclic behavior repeated in the same way until production stopped. As mentioned in Section 3.2.2, the upward flow propagated the change of h_{mix} to the shallower part of the wellbore. This propagation altered the density profile and ρ_{aves}, inducing cyclic discharge.

Figure 8 shows profiles of density and specific enthalpy in the well with time during t = 17200–21000 s. As high specific enthalpy (1135 kJ/kg) propagated from FZs after 17500 s, the water single-phase column in the shallower part of the wellbore moved upward and its bottom separated from FZs. This column shortened with time and disappeared at 19300 s. Then, a water single phase formed again at FZs and the high-enthalpy fluid flowed upward rapidly. From the figure, the density decreased along high-enthalpy paths, which occurred from FZs to the wellhead.

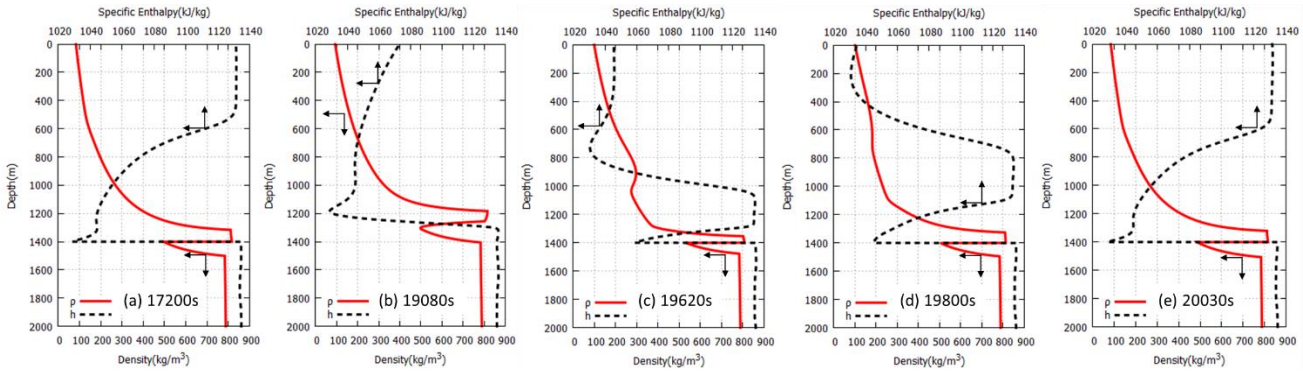

Figure 7: Profile of specific enthalpy and density in the well at 17200, 19080, 19620, 19800, and 20030 s

3.2.7 Relationship between average density in shallow part of the wellbore and density profile

Figure 9(a) shows density at depths 0, 600, 1200 and 1400 m and ρ_{aves} with time. All the densities oscillated but their amplitudes varied; it was 508.3 kg/m^3 at depth 1200 m but just 18.9 kg/m^3 at the wellhead. Figure 9(b) shows the relationship between density and pressure with time at depths 0, 600, 1200, 1400 and 1600 m. This figure represents the locus of density and pressure at each depth. The orange solid line shows the relationship between density and pressure at 1135 kJ/kg. The locus at depth 1600m forms a straight line along the orange solid line. This is because 1600 m is deeper than FZs so that specific enthalpy remained constant at 1135 kJ/kg, and density and pressure were unique as mentioned in Section 3.2.2. In contrast, the locus at depth 1400 m forms a curve and part of it does not coincide with the orange solid line. When P_{fzs} was < 45 bar, different enthalpy fluids mixed at FZs so that h_{mix} changed as described by Eq. (14). Moreover, P_{fzs} and h_{mix} are unique as mentioned in Section 3.2.5 so that the locus at 1400 m depth forms a single curve. Unlike those two loci, loci at depths 1200 and 600 m form spirals. These loci start at the center of the spiral and rotate clockwise as its radius increases with time. This is because P and h are not unique and their amplitude gradually increases with time, owing to the propagation of h from FZs and change of ρ_{aves}. The orange dotted line shows the relationship between density and pressure at 1024 kJ/kg. This specific enthalpy is the minimum h_{mix} during the oscillation, so that all loci are between the solid and dotted orange lines. Here, saturation pressures of water for 1024 and 1135 kJ/kg are 31.8 and 47.0 bar, respectively, and the pressure difference is 15.2 bar. This pressure difference indicates that the depth where pressure is between 31.8 and 47.0 bar can have both water single-phase and two-phase between 1100 and 1400 m depths, so the range of density can be large relative to that at shallow depths from 0 to 600 m. Therefore, ρ_{aves} is strongly affected by the density change between depths 1100 and 1400 m.

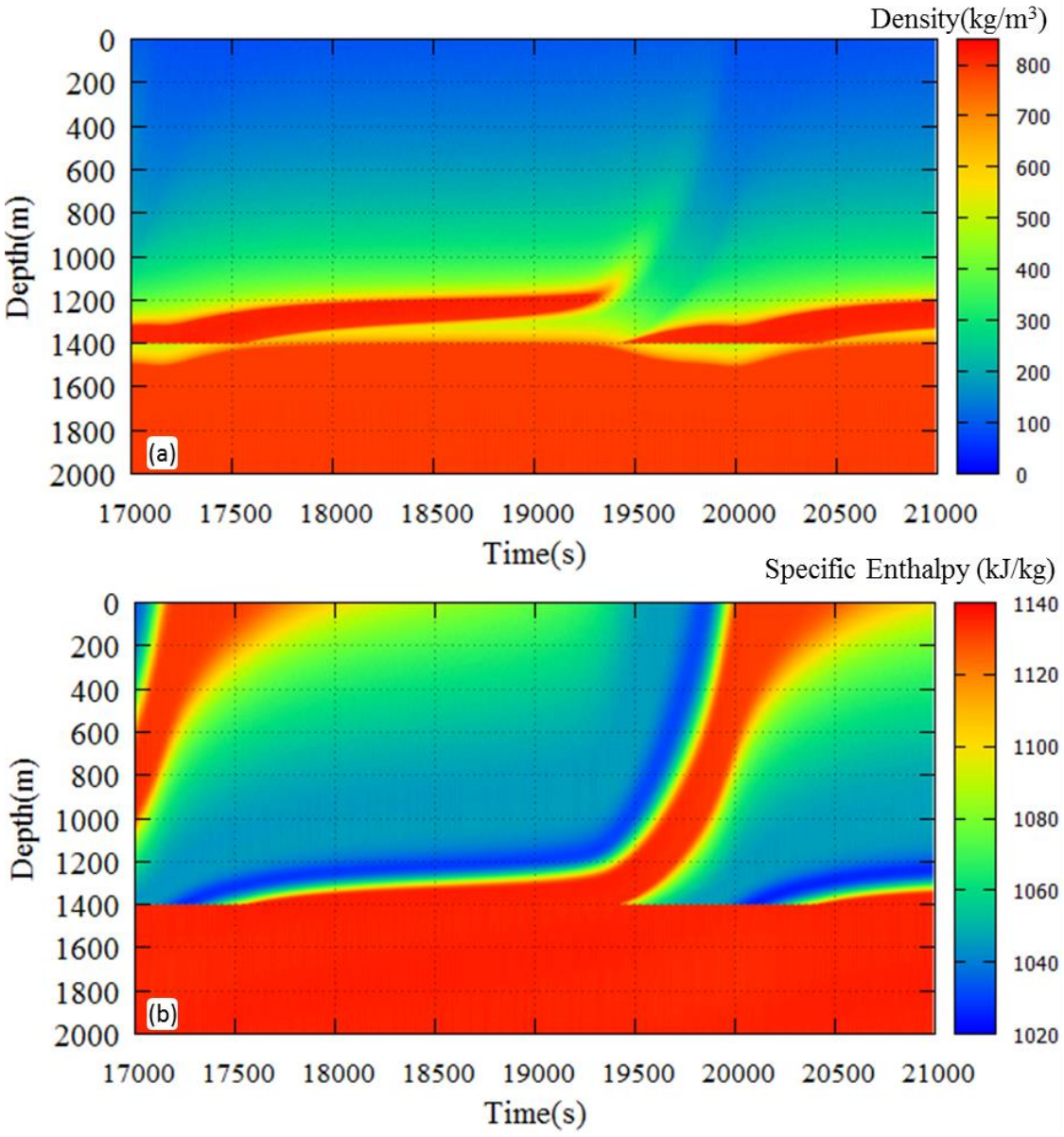

Figure 8: Profiles as a function of time during 17000–21000 s: (a) Density; (b) specific enthalpy

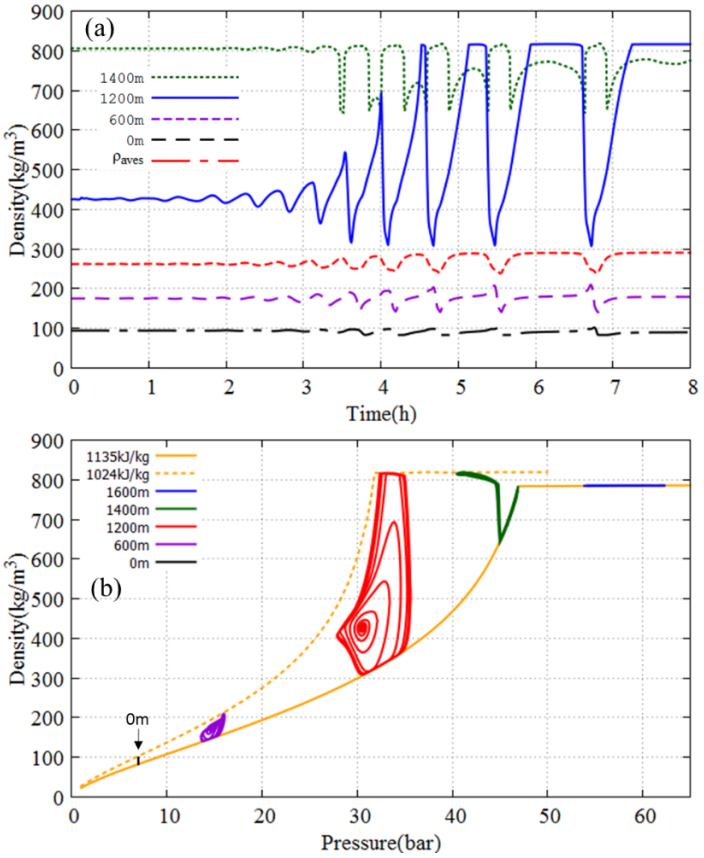

Figure 9: (a) Change of density at depths 0, 600, 1200 and 1400 m, and ρ_{aves} with time; (b) Density versus pressure at depths 0, 600, 1200, and 1400 m with time and density versus pressure at 1135 and 1024 kJ/kg

3.2.8 Criteria for production stop

As mentioned in Section 3.2.1, production ceased after the unstable behavior. Figure 10 shows flow rates M_{fzs} and M_{fzd} and total flow rate M_t with time. All flow rates were positive early. M_{fzs}, however, become negative after 3.5 h during the oscillation, so that part of M_{fzd} flowed out to the shallow reservoir from the wellbore at FZs. Then, all of M_{fzd} flowed out to that reservoir after 7 h and M_t became 0 and production halted. This relationship is represented by

$$M_t = M_{fzs} + M_{fzd} = 0. \tag{20}$$

Three situations can satisfy this condition: 1) Both flow rates are zero; 2) all of M_{fzs} flows out to the deep reservoir; 3) all of M_{fzd} flows out to the shallow reservoir. Our simulated results show that productions stopped because the third condition was satisfied.

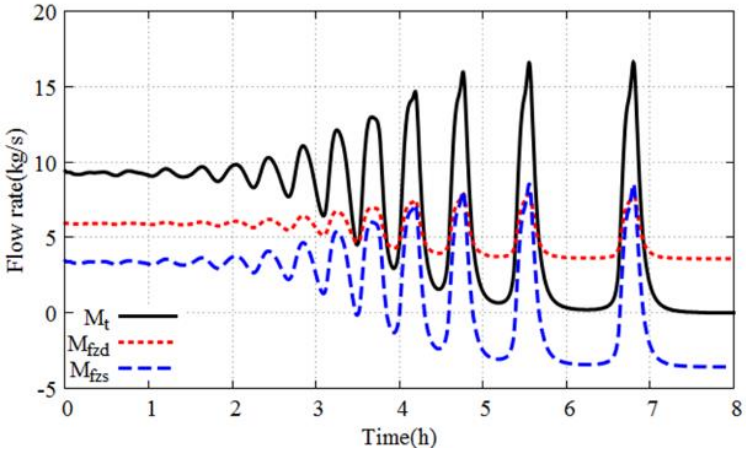

Figure 10: Changes of M_{fzs}, M_{fzd}, and M_t with time

4. MECHANISM OF UNSTABLE BEHAVIOR

We discussed the mechanism of unstable behavior in the well. Figure 11 shows a schematic of the cycle of unstable behavior. We assumed that ρ_{aves} and P_{fzs} increased with time. This pressure increase reduced M_{fzs} and Rs and increased h_{mix}. The latter increase propagated toward the shallower part of the wellbore because of the upward flow, and specific enthalpy gradually increased as high specific enthalpy fluid flowed upward. Then, density decreased where this high enthalpy fluid reached. This continuous decrease in density in the shallower part of the wellbore decreased ρ_{aves} over time. This induced a decrease in P_{fzs}, increase in M_{fzs} and Rs, and decrease in h_{mix}. Low-enthalpy fluid flowed upward and density in the shallower part of the wellbore increased. Consequently, ρ_{aves} began to increase again, and the oscillation repeated. In the calculation, the amplitude of P_{fzs} rose gradually and all of M_{fzd} flowed out to the shallow reservoir so that the production and oscillation finally ceased.

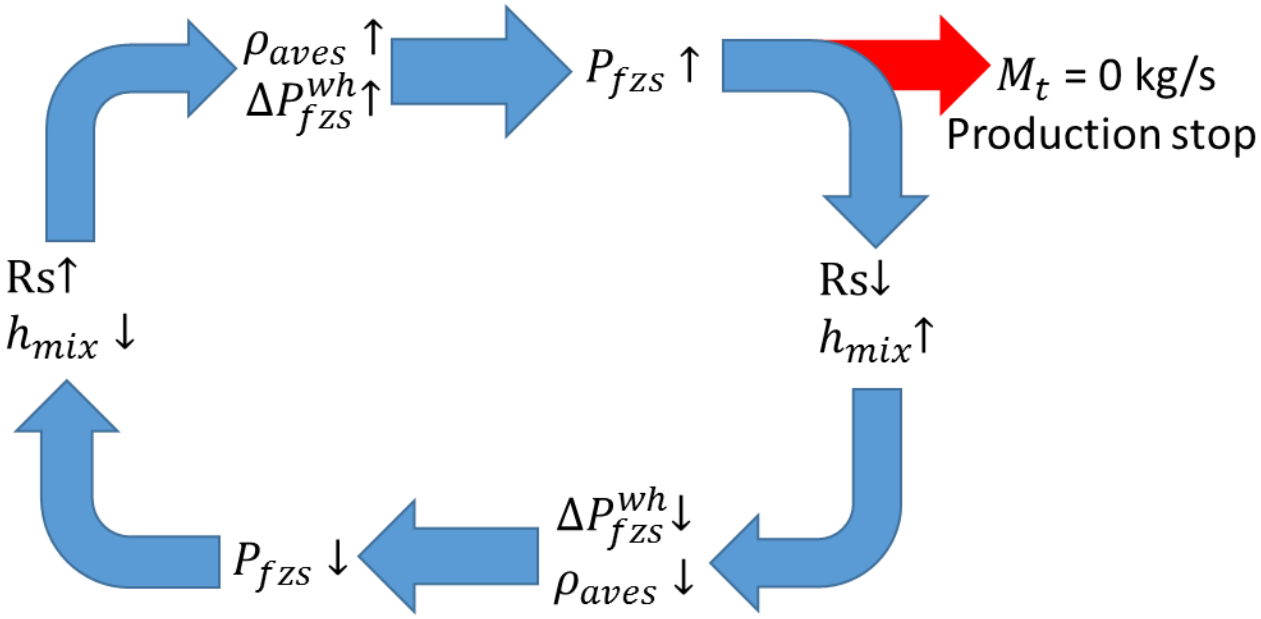

Figure 11: Mechanism of the cyclic discharge

5. FLOW INSTABILITY BOUNDARY MAP

In Sections 3 and 4, we indicated that the unstable flow occurred when ΔT_{re} was large. In this section, we examine the effects of permeability thickness of the shallow and deep reservoir, kh_s and kh_d, on the unstable flow. Reservoir parameters are summarized in Table 2. Other simulation conditions were the same as in Section 3. The calculation was done for each condition and we determined whether the simulation result showed unstable behavior.

Table 2: Parameters of each reservoir

Reservoir	Depth(m)	Pressure(bar)	Temperature (°C)	kh (darcy·m)	Outer radius (m)
Deep	2000	100	260	1.0	1000
Shallow	1400	45	160～250	1.0~10.0	1000

Figure 12 shows the flow instability boundary map for variable kh_s and T_{res}. The blue circles and red triangles represent the condition of kh_s and T_{res} that shows stable behavior as in Fig. 2(a) and unstable behavior as in Fig. 2(b), respectively. T_{res} = 226 °C was the boundary of stable and unstable behavior when kh_s = 4 darcy・m. The black line is the boundary between stable and unstable results. This curve represents the boundary of T_{res}, which shows unstable flow changes with kh_s. Unstable behavior occurred even for high T_{res}, and the temperature difference between feed zones was small with an increase in kh_s. Parameters of the deep reservoir were fixed in these calculations so that the relationship of P_{fzs} and P_{fzd} is given by Eq. (13). Figure 13(a) and (b) portray the relationship between P_{fzs}, Rs, and absolute value of the derivative (Rs') of Rs for T_{res} = 220 °C and kh_s = 1, 4, and 10 darcy・m. These curves show that Rs increased with kh_s, and Rs' also increased with kh_s when P_{fzs} was close to 45 bar. As mentioned in Section 3, h_{mix} increased with a decrease in P_{fzs} because of change in Rs, and this change of h_{mix} caused the cyclic discharge. Figure 13(a) and (b) reveal that Rs and Rs' increased with kh_s so that the influence of P_{fzs} on h_{mix} also increased with kh_s. Therefore, when kh_s was sufficiently large, there was unstable behavior even when T_{res} was high and ΔT_{re} was small.

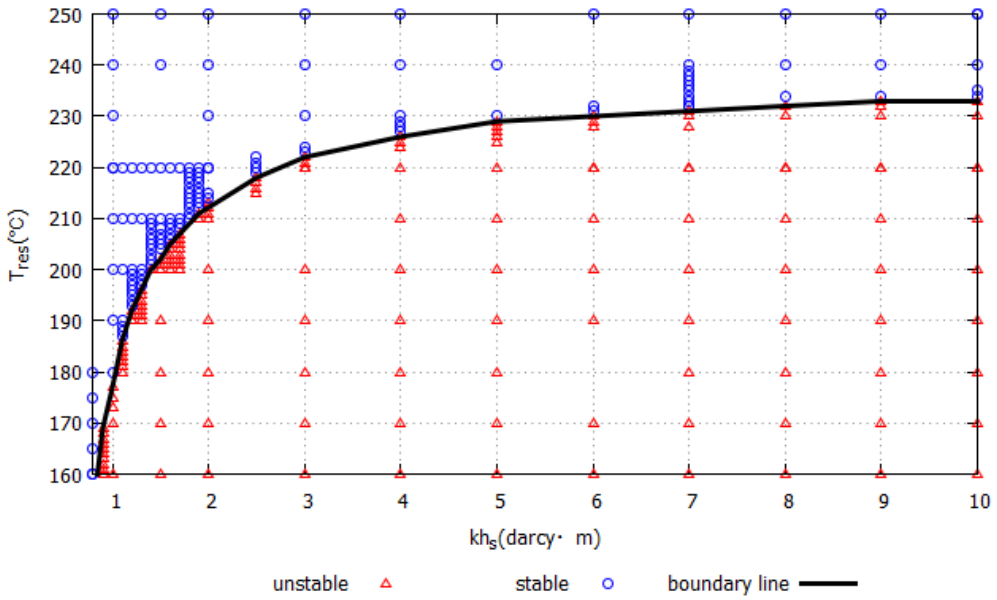

Figure 12: Flow instability boundary map

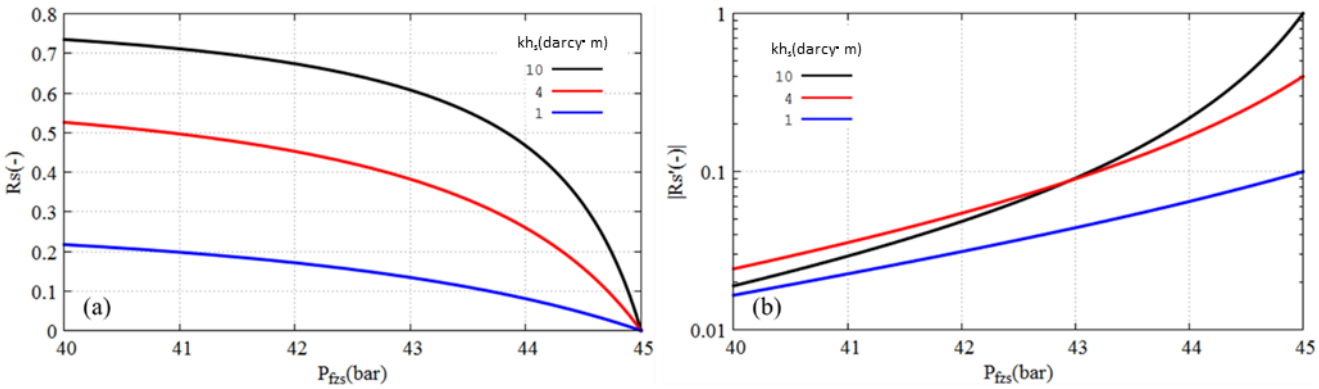

Figure 13: (a) Rs versus P_{fzs} when kh_s = 1, 4, and 10 darcy・m; (b) Rs' versus P_{fzs} when kh_s = 1, 4, and 10 darcy・m

5. CONCLUSIONS

1. We developed a numerical simulator for unstable water-steam two-phase flow in the wellbore with multiple feed zones.

2. Simulation results show that wellbore flow became unstable when the temperature difference between the two reservoirs was substantial.

3. Production stopped following the unstable behavior, because the total flow rate of upward flow from FZs became zero during the oscillation.

4. The mechanism of the unstable behavior is understood by considering interactions between the propagation of h_{mix} to the shallow part of the wellbore, average density between the wellhead and FZs, and pressure loss in the wellbore.

5. The oscillation was strongly affected by phase change at depths where there could be both water single-phase and two-phase, because of the specific enthalpy change. This condition was not found in the shallower part of the wellbore from 0 to 600 m, but in the deeper part, from 1100 to 1400 m.

6. The flow instability boundary map was constructed, and it shows that unstable behavior readily occurred with an increase in kh_s, even for high T_{res} and a small temperature difference between feed zones.

REFERENCES

Brill, J.P., and Mukherijee, H.: Multiphase Flow in Wells, SPE Monograph Series, Society of Petroleum Engineers Inc., Richardson, TX, USA, (1999), 77 pp.

Grant, M.A., Bixley, P.F., and Syms, M.C.: Instability in Well Performance, *Geothermal Resources Council*, **3**, (1979), 275-278.

Inagaki, H., Itoi, R., Kumagai, N., and Iwasaki, T.: Numerical Simulation on Fluctuation in Wellhead Pressure of Geothermal Well, *Proceedings*, Stanford Geothermal Workshop (2014).

Itoi, R., Katayama, Y., Tanaka, T., Kumagai, N., and Iwasaki, T.: Numerical Simulation of instability of geothermal production well, *Geothermal Resources Council Transactions*, **37**, (2013), 837-841.

Iwata, S., Nakano, Y., Granados, E., Butler, S., and Tait, A.R.: Mitigation of Cyclic Production Behavior in a Geothermal Well at the Uenotai Geothermal Field, Japan. *Geothermal Resources Council Transactions*, **26**, (2002), 193-196.

Japan Society of Mechanical Engineers: Fluid Resistance of Pipes and Ducts (in Japanese), *Maruzen* (1979).

Katayama, Y., Itoi, R., Kumagai, N. and Iwasaki, T.: Flow Characteristics of Geothermal Production Well with Multi-Feed Zones, *Geothermal Resources Council Transactions*, **35**, (2011), 1475-1479.

Katayama, Y., Itoi, R., and Tanaka, T.: Numerical Simulation of Transient Two-phase Flow in Geothermal Production Well with Multi-feed Zones, *Proceedings*, 2nd ITB Geothermal Workshop (2013).

Miller, C.: Wellbore User's Manual, Lawrence Berkley Laboratory, University of California, (1980), 48 pp.

Nakayama, Y.: "The mechanics of fluid" (in Japanese), Youkendo (2007).

Pan, L., Oldenburg, C. M., Wu, Y., and Pruess, K.: Wellbore Flow Model for Carbon Dioxide and Brine, *Energy Procedia*, **1**, (2009), 71-78.

Pan, L., and Oldenburg, C. M.: T2Well-An Integrated Wellbore-Reservoir Simulator, *Computers & Geosciences*, **65**, (2014), 46-55.

Pruess, K.: On CO2 Fluid and Heat Transfer Behavior in the Subsurface, Following Leakage from a Geologic Storage Reservoir, *Environmental Geology*, **54**, (2008), 1677-1686.

Smith, S. L.: Void Fractions in Two-Phase Flow: A Correlation Based upon an Equal Velocity Head Model, *Proceedings*, Institution of Mechanical Engineers (1969-70).

Yamamura, K., Itoi, R., Tanaka, T., and Iwasaki T.: Numerical Model of Unsteady Two-Phase Flow in Geothermal Production Well, *Proceedings*, 5th ITB International Geothermal Workshop (2016).